Epitaxial Mn_2VAl films with $L2_1$-ordered structure for all-Heusler stacks

Shinya Yamada[a,b], Kohei Kudo[b], Ryosuke Sadakari[b], Kohei Hamaya[a,b]

[a] *Center for Spintronics Research Network, Osaka University, Toyonaka, Osaka 560-8531, Japan*
[b] *Graduate School of Engineering Science, Osaka University, Toyonaka, Osaka 560-8531, Japan*

Abstract

The structural and magnetic properties of epitaxial Mn_2VAl films grown by molecular beam epitaxy are investigated. Epitaxial Mn_2VAl films with a relatively high $L2_1$-ordering of ∼0.7 are obtained on MgO(001) substrates at a growth temperature of 350 °C. The saturation magnetic moment at 300 K for the epitaxial Mn_2VAl films is ∼1.2 μ_B/f.u., which is almost equivalent to the highest value for high-temperature-grown thin-film samples reported previously. Due to the low-temperature synthesis of $L2_1$-Mn_2VAl, an epitaxial all-Heusler $L2_1$-Mn_2VAl/$L2_1$-Fe_2VAl/$L2_1$-Mn_2VAl trilayer with sharp heterointerfaces is obtained. This study presents the possibility of all-Heusler current-perpendicular-to-plane giant magnetoresistive devices with high performance.

Keywords: Heusler alloy, Mn_2VAl, Epitaxial films, Molecular beam epitaxy

1. Introduction

Full-Heusler alloys with a chemical formula of X_2YZ (X, Y: transition metals; Z: a main group element) have been widely studied because of their potential for various functionalities[1–3]. In particular, half-metallic full-Heusler alloys have been explored as ferromagnetic electrodes for the tunneling magnetoresistance effect[4, 5], the current-perpendicular-to-plane giant magnetoresistance (CPP-GMR) effect[6, 7], and spin injection into semiconductors[8–12].

Among the full-Heusler alloys with a half-metallic nature and a high Curie

temperature, a ferrimagnetic Heusler alloy, Mn_2VAl[13, 14], has been focused on as a potential spintronic material. The Mn and V atoms in $L2_1$-ordered Mn_2VAl are antiferromagnetically coupled (Mn: 1.413 μ_B/f.u.; V: -0.786 μ_B/f.u.)[14]. Therefore, Mn_2VAl has a small magnetic moment ($\sim$2 μ_B/f.u.)[14] compared with well-known half-metallic full-Heusler alloys such as Co_2MnSi ($\sim$5 μ_B/f.u.)[15] and Co_2FeSi ($\sim$6 μ_B/f.u.)[16]. Because the critical current density required to switch the magnetization through the spin-transfer torque is proportional to the product of the saturation magnetization (M_S)[17], the use of $L2_1$-ordered Mn_2VAl as a ferromagnetic electrode in spintronic devices has an advantage in terms of low-power-consumption magnetization switching. In addition, $L2_1$-ordered Mn_2VAl shows a high Curie temperature of 760 K in the bulk[18], which is suitable for practical applications. Furthermore, a theoretical study has proposed that $Mn_2VAl/Fe_2VAl/Mn_2VAl$ all-Heusler-based CPP-GMR junctions would exhibit a significantly large output due to the band symmetry and Fermi surface matching[19]. Therefore, Mn_2VAl has significant potential as a spintronic material in terms of device applications.

Many experimental studies on Mn_2VAl have been reported for the bulk[18, 20–25] and thin films[26–32]. A high degree of $L2_1$-ordering (S_{L2_1}) of $\sim$0.84 and an almost theoretical M_S value of $\sim$1.82 μ_B/f.u. at 5 K were reported for bulk samples[25]. In contrast, the values of S_{L2_1} and M_S for thin-film samples were much smaller than those for the bulk samples[26–28]. Relatively high S_{L2_1} and M_S values were recently reported for thin-film samples[29, 30]. However, a high growth temperature (T_g) above 500 °C is generally required to obtain $L2_1$-ordered Mn_2VAl films[26–30, 32]. Since such a high T_g can easily induce atomic interdiffusion in spintronic devices, there are some limitations to its applications such as the all-Heusler-based CPP-GMR devices.

We have developed techniques for the growth of some full-Heusler alloys by low-temperature molecular beam epitaxy (MBE). Unlike most thin-film studies on full-Heusler alloys, relatively high degrees of structural ordering have been obtained at less than 350 °C[10, 12, 33–44]. These low-temperature MBE techniques have also enabled all-Heusler stacks with sharp heterointerfaces[45, 46].

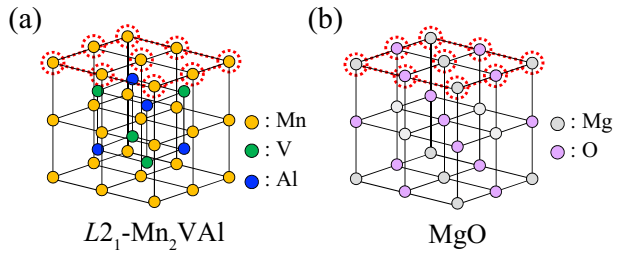

Figure 1: (Color online) Schematics of crystal structure and atomic arrangements of the (001) plane for (a) $L2_1$-ordered Mn_2VAl and (b) MgO.

If the low-temperature synthesis of $L2_1$-ordered Mn_2VAl can be achieved, then various spintronic applications can be expected.

In this paper, we study the structural and magnetic properties of epitaxial Mn_2VAl films grown by MBE. Epitaxial Mn_2VAl films with a relatively high S_{L2_1} of ∼0.7 are obtained on MgO(001) substrates at a T_g of 350 °C. The value of M_S at 300 K for the epitaxial Mn_2VAl films is ∼1.2 μ_B/f.u., which is almost equivalent to the highest value for high-temperature-grown thin-film samples reported previously[29]. Due to the low-temperature synthesis of $L2_1$-Mn_2VAl, an epitaxial all-Heusler $L2_1$-Mn_2VAl/$L2_1$-Fe_2VAl/$L2_1$-Mn_2VAl trilayer with sharp heterointerfaces is obtained.

2. Experimental methods

Before investigating the crystal growth, we explain the crystal structures of Mn_2VAl and MgO, which are illustrated in Figs. 1(a) and 1(b), respectively. The mismatch between the lattice constant of Mn_2VAl (0.587 nm) and the diagonal length of the lattice constant of MgO ($\sqrt{2}$×0.422 nm = 0.597 nm) is ∼1.7%. The atomic arrangement in the (001) plane between Mn_2VAl and MgO is matched, as shown by the dotted lines in Figs. 1(a) and 1(b). Therefore, an epitaxial relationship of Mn_2VAl[100](001)//MgO[110](001) can be expected.

Mn_2VAl films were grown on MgO(001) substrates by MBE[41, 47]. After heat treatment was performed at 500 °C for 1 h, good flatness of the MgO(001)

surface was confirmed by in situ reflection high-energy electron diffraction (RHEED) observations[41, 47]. Cooling the substrate temperature to 100 or 350 °C, Mn_2VAl films with a thickness of ∼25 nm were grown by co-evaporating Mn, V, and Al using Knudsen cells. Here we set the atomic composition ratio of Mn:V:Al to 2:1.2:2 during growth because the stoichiometric deposition causes deviation of the film composition from stoichiometry under the MBE conditions employed. Structural characterization was conducted using in situ RHEED observations, X-ray diffraction (XRD), high-angle annular dark-field scanning transmission electron microscopy (HAADF-STEM), and energy-dispersive X-ray spectroscopy (EDX) measurements. Magnetic properties were measured with a vibrating sample magnetometer in a physical property measurement system (Quantum Design).

3. Results and discussion

Figures 2(a) and 2(b) show in situ RHEED images of Mn_2VAl films grown at 100 and 350 °C, respectively. Symmetrical streaks, which indicate two-dimensional epitaxial growth, are observed for both samples. In particular, for the sample grown at 350 °C, half-order streaks are observed in the RHEED image (yellow arrows), which indicates the formation of the $L2_1$-ordered structure.

Figure 2(c) shows XRD profiles by ω-2θ scan for the Mn_2VAl films. 004 diffraction peaks of Mn_2VAl are observed for both samples, which indicates the formation of (001)-oriented epitaxial Mn_2VAl films. The values of the lattice constant estimated from the XRD data for the samples grown at 100 and 350 °C were 0.588 and 0.587 nm, respectively, which are equivalent to those for bulk[18] and thin-film[26, 28–30] samples reported previously. For the sample grown at 350 °C, 002 superlattice diffraction of Mn_2VAl due to the presence of a $B2$-ordered structure is observed. In contrast, for the sample grown at 100 °C, only the 004 diffraction peak of Mn_2VAl is observed, which indicates that this Mn_2VAl film forms an $A2$ structure. From ϕ-scan measurements of the

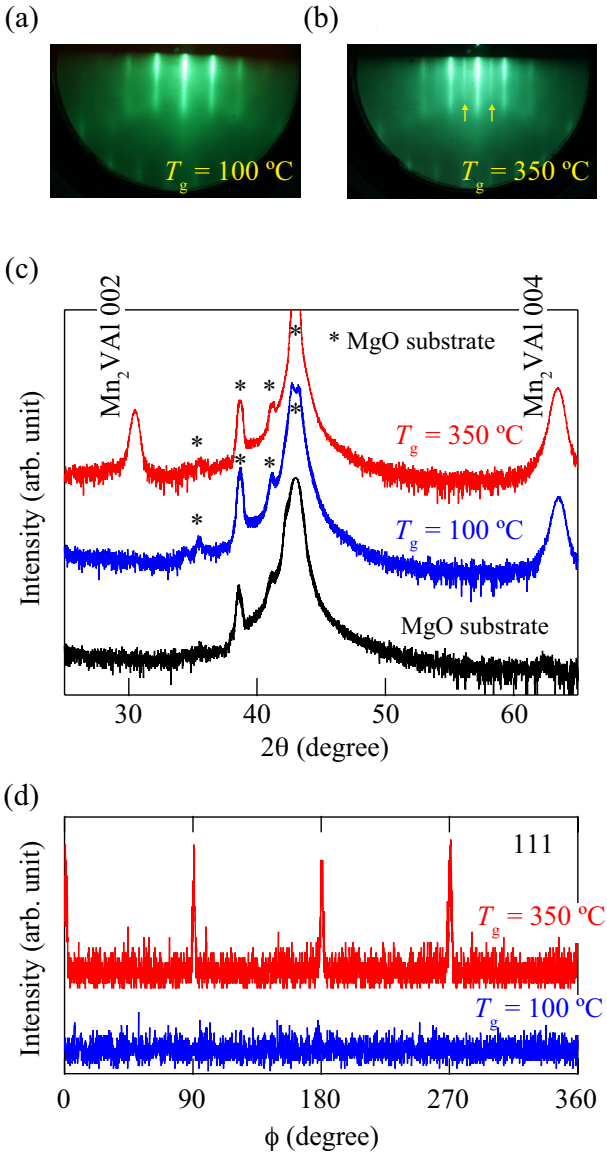

Figure 2: (Color online) RHEED images of Mn_2VAl films grown at (a) 100 and (b) 350 °C. (c) XRD profiles by ω-2θ scan for Mn_2VAl films, together with that for a MgO(001) substrate. (d) XRD ϕ-scan measurement of the (111) plane for Mn_2VAl films.

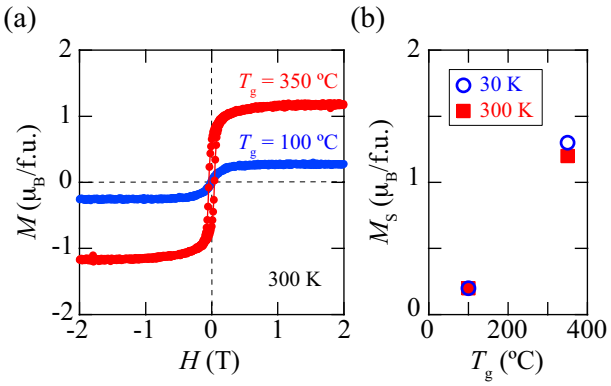

Figure 3: (Color online) (a) In-plane M-H curves measured at 300 K and (b) M_S versus T_g for the Mn_2VAl films.

(202) plane for the Mn_2VAl layer and the MgO substrate (not shown here), we confirmed an in-plane crystal orientation of Mn_2VAl[100](001)//MgO[110](001) for both samples. The ϕ-scan measurements of the (111) plane are shown in Fig. 2(d). Sharp diffraction peaks with fourfold symmetry are observed only for the sample grown at 350 °C, which indicates the presence of the $L2_1$-ordered structure in the film. The degree of $B2$ and $L2_1$ ordering, S_{B2} and S_{L2_1}, is estimated from the XRD data for the Mn_2VAl film grown at 350 °C using the following equations [48, 49],

$$S_{B2} = \sqrt{\frac{I_{002}/I_{004}}{I^R_{002}/I^R_{004}}}, \quad S_{L2_1} = \frac{2}{3 - S_{B2}} \sqrt{\frac{I_{111}/I_{202}}{I^R_{111}/I^R_{202}}}, \tag{1}$$

where I_{hkl} and $I^R{}_{hkl}$ are the experimental and theoretical peak intensities for the hkl plane, respectively. The values of S_{B2} and S_{L2_1} were thus estimated to be ∼1 and ∼0.7, respectively. Although the T_g of 350 °C in this study is lower than those reported in previous thin-film studies[26, 28, 29], a relatively high S_{L2_1} value is obtained. In addition, the value of S_{B2} for the film grown at 350 °C is ∼1, which indicates that $B2$-type disorder is suppressed under the MBE growth conditions.

Figure 3(a) shows in-plane field-dependent magnetization (M-H curves) at 300 K for the Mn_2VAl films, where the magnetic field was applied along [110]

Table 1: Comparison of S_{L2_1} and M_S for bulk and thin-film Mn_2VAl. [25, 26, 28–30]

Sample	Method	S_{L2_1}	M_S (μ_B/f.u.)
Poly-crystalline bulk[25]	Arc melting (1200 °C)	∼0.84	∼1.82 (5 K)
Epitaxial film[26]	Sputtering (T_g = 500 °C)	∼0.5 ($S_{B2} \sim 0.5$)	∼0.81 (10 K), ∼0.54 (300 K)
Epitaxial film[28]	Sputtering (T_g = 700 °C)	∼0.4 ($S_{B2} \sim 0.7$)	∼0.88 (20 K)
Epitaxial film[29]	Sputtering (T_g = 600 °C)	∼0.77 ($S_{B2} \sim 0.79$)	∼1.3 (300 K)
Epitaxial film[30]	Sputtering (T_g = 600 °C)	∼0.66 ($S_{B2} \sim 0.74$)	∼1.2 (300 K)
Epitaxial film (This work)	MBE (T_g = 350 °C)	∼0.7 ($S_{B2} \sim 1$)	∼1.3 (30 K), ∼1.2 (300 K)

direction of Mn_2VAl. The value of M_S at 300 K for the sample grown at 350 °C is estimated to be ∼1.2 μ_B/f.u., which is comparable to those for high-temperature-grown thin-film samples[29]. The coercivity of ∼40 mT is equivalent to those for the high-temperature-grown thin-film samples[29]. In contrast, for the sample grown at 100 °C, the value of M_S at 300 K is only ∼0.2 μ_B/f.u. due to formation of the $A2$ structure in the films[26, 28, 29]. Figure 3(b) shows the values of M_S at 30 and 300 K versus T_g for the Mn_2VAl films. The values of S_{L2_1} and M_S for bulk[25] and thin-film[26, 28, 29] Mn_2VAl are summarized in Table I. While high T_g above 500 °C is typically required to obtain high S_{L2_1} and M_S values[25, 29], relatively high S_{L2_1} and M_S values are obtained at 350 °C in our MBE conditions. However, while the values of S_{B2} and S_{L2_1} in our 350 °C-grown films are ∼1 and ∼0.7, the value of M_S remains 60% of the theoretical value[14]. As described later, the chemical composition of the Mn_2VAl layer on MgO(001) is almost stoichiometric, so that we expect that influence of excess V atoms in our Mn_2VAl films on the reduction in M_S is small. Although the $D0_3$-type disorder also affects the value of M_S in Mn_2VAl, it is generally difficult to quantitatively evaluate the degree of the $D0_3$ disordering from a conventional XRD apparatus. At present, although there is still room to improve the S_{L2_1} and M_S values in our Mn_2VAl films, the results indicate the potential for the low-temperature synthesis of thin-film Mn_2VAl with high S_{L2_1} and high M_S under the as-grown conditions.

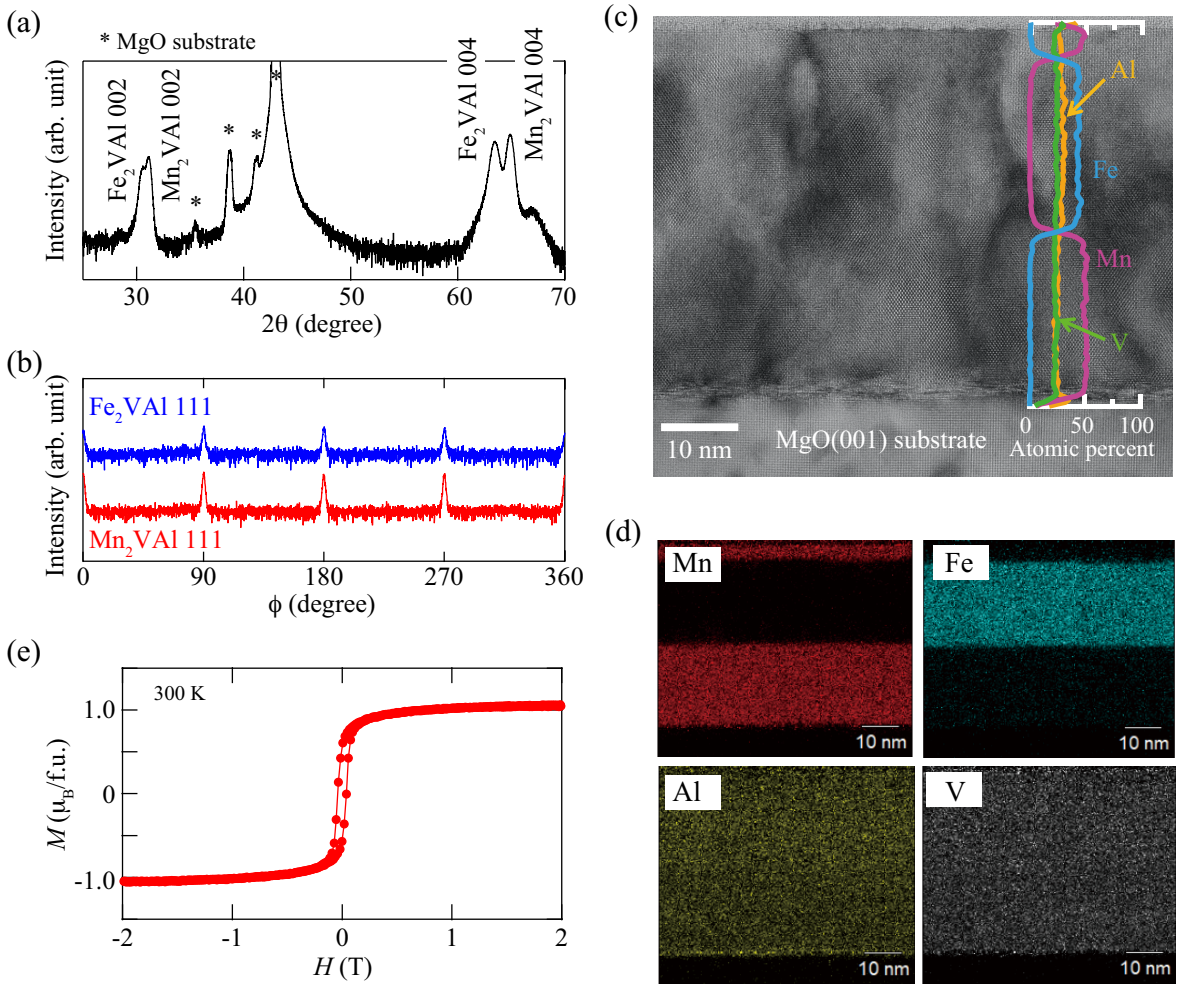

Figure 4: (Color online) (a) XRD profiles by ω-2θ scan for a $Mn_2VAl/Fe_2VAl/Mn_2VAl$ trilayer on MgO(001). (b) XRD ϕ-scan measurement of the (111) plane of Fe_2VAl (blue) and Mn_2VAl (red) for trilayer. (c) HAADF-STEM image and EDX line profiles for the trilayer. (b) EDX elemental maps of the region shown in (d).(e) In-plane M-H curve measured at 300 K for the trilayer.

Finally, we attempted to grow a $Mn_2VAl/Fe_2VAl/Mn_2VAl$ trilayer on a MgO(001) substrate, where $L2_1$-ordered Fe_2VAl is a well-known nonmagnetic Heusler alloy[39, 50]. The thicknesses of the top-Mn_2VAl, Fe_2VAl spacer, and bottom-Mn_2VAl layers were ∼15, ∼20, and ∼25 nm, respectively. During the growth of the trilayer, the substrate temperature was fixed to be 350 °C and we did not perform post-annealing after the growth of each layer. The detailed growth conditions for the Fe_2VAl spacer layer are given in our previous studies[39, 40, 51]. After the growth of each layer, symmetrical streaks, which indicate two-dimensional epitaxial growth, were observed. Figure 4(a) shows an XRD profile by ω-2θ scan for the $Mn_2VAl/Fe_2VAl/Mn_2VAl$ trilayer on MgO(001). 002 and 004 diffraction peaks of Mn_2VAl and Fe_2VAl are observed. From the ϕ-scan measurements of the (111) plane of Mn_2VAl and Fe_2VAl shown in Fig. 4(b), we can confirm the presence of $L2_1$-ordered structures in the Mn_2VAl and Fe_2VAl layers.

Figure 4(c) shows a HAADF-STEM image and EDX line profiles for the $Mn_2VAl/Fe_2VAl/Mn_2VAl$ trilayer on MgO(001). The interfaces among the top Mn_2VAl, Fe_2VAl spacer, and bottom Mn_2VAl layers cannot be identified from the HAADF-STEM image. From the EDX line profiles, the chemical composition along the stacking direction is abruptly changed at ∼25 and ∼40 nm from the MgO(001) substrate. For the bottom Mn_2VAl layer, the chemical composition is confirmed to be stoichiometric (Mn:V:Al = 2:1:1), even though we used nonstoichiometric deposition conditions. Although the actual chemical composition in the Fe_2VAl spacer layer (Fe:V:Al = 1.8:1.0:1.2) and top-Mn_2VAl layer (Mn:V:Al = 1.8:1.0:1.2) slightly deviates from the stoichiometry, no atomic interdiffusion is evident from the EDX elemental maps shown in Fig. 4(d). From the HAADF-STEM image in Fig. 4(c), the presence of an $L2_1$-ordered structure in each Heusler-alloy layer is confirmed.

An in-plane M-H curve at 300 K for the trilayer is shown in Fig. 4(e), where the magnetic field was applied along [110] direction of Mn_2VAl. Here we assume that the Fe_2VAl spacer layer is nonmagnetic because the values of M_S for highly ordered epitaxial Fe_2VAl films are negligible small[39, 52]. The value

of M_S for the Mn_2VAl layers in the trilayer is estimated to be $\sim$1.1 μ_B/f.u., which is equivalent to that for the single Mn_2VAl layer shown in Fig. 3(a). We speculate that the slight reduction in M_S from Fig. 3(a) is caused by the Al-rich composition in the top-Mn_2VAl layer.

We have determined that epitaxial Mn_2VAl films with a relatively high S_{L2_1} can be obtained by MBE at a low T_g of 350 °C. It is noted that the values of S_{B2} and S_{L2_1} for the epitaxial Mn_2VAl films in this study were almost equivalent to those for the epitaxial Fe_2VAl films reported in our previous studies[39, 40]. Although there is only a difference in constituent elements at the (A,C) sites between $L2_1$-Mn_2VAl and $L2_1$-Fe_2VAl, the value of S_{B2} was $\sim$1 for both the Mn_2VAl and Fe_2VAl films. This indicates that the low-temperature MBE enables the suppression of Mn$\Leftrightarrow$V disordering or Fe$\Leftrightarrow$V disordering during growth. As a result, we have achieved an all-Heusler stack with $L2_1$-ordered structures and the sharp heterointerfaces shown in Fig. 4(c).

While many theoretical studies on the electronic band structures and magnetic properties of all-Heusler stacks have been reported[19, 53–64], there has only been a few experimental studies[45, 46, 65, 66]. In particular, for the emergence of unique physical properties expected theoretically, it is necessary to precisely control the structural ordering in not only the bulk region but also the interfacial region of all-Heusler stacks. From the structural characterization and magnetic property measurements, we have confirmed that there is still room to improve the structural characteristics of the all-Heusler stack shown in Fig. 4(c). To realize high-performance CPP-GMR devices due to the band symmetry and Fermi surface matching[19, 67, 68], improvement of the crystal quality of the trilayer and reduction of the Fe_2VAl spacer layer thickness should be investigated.

4. Conclusion

We have studied the structural and magnetic properties of epitaxial Mn_2VAl films grown by MBE. The MBE technique enabled epitaxial Mn_2VAl films with

relatively high S_{L2_1} and M_S values to be grown at a T_g of 350 °C. These S_{L2_1} and M_S values were comparable to those for high-temperature-grown thin-film samples reported previously. Due to the low-temperature synthesis of $L2_1$-Mn_2VAl, an all-epitaxial $L2_1$-Mn_2VAl/$L2_1$-Fe_2VAl/$L2_1$-Mn_2VAl trilayer with sharp heterointerfaces, where Mn_2VAl/Fe_2VAl junctions are theoretically expected to exhibit high magnetoresistive properties, was obtained.

5. Acknowledgments

This work was supported in part by JSPS KAKENHI Grant Numbers 19H05616, 20J10124, the Nippon Sheet Glass Foundation for Materials Science and Engineering, the Hitachi Metals and Materials Science Foundation, and the Spintronics Research Network of Japan (Spin-RNJ).

References

[1] F. Heusler, Verh. Dtsch. Phys. Ges. 12 (1903) 219.

[2] K. Manna, Y. Sun, L. Muechler, J. Kübler, and C. Felser, Nat. Rev. Mater. 3 (2018) 244.

[3] K. Elphick, W. Frost, M. Samiepour, T. Kubota, K. Takanashi, H. Sukegawa, S. Mitani and, A. Hirohata, Sci. Technol. Adv. Mater. 22 (2020) 235.

[4] Y. Sakuraba, M. Hattori, M. Oogane, Y. Ando, H. Kato, A. Sakuma, T. Miyazaki, H. Kubota, Appl. Phys. Lett. 88 (2006) 192508.

[5] R. Shan, H. Sukegawa, W. H. Wang, M. Kodzuka, T. Furubayashi, T. Ohkubo, S. Mitani, K. Inomata, and K. Hono, Phys. Rev. Lett. 102 (2009) 246601.

[6] K. Yakushiji, K. Saito, S. Mitani, and K. Takanashi, Y. K. Takahashi and K. Hono, Appl. Phys. Lett. 88 (2006) 222504.

[7] T. Furubayashi, K. Kodama, H. Sukegawa, Y. K. Takahashi, K. Inomata, and K. Hono, Appl. Phys. Lett. 93 (2008) 122507.

[8] T. A. Peterson, S. J. Patel, C. C. Geppert, K. D. Christie, A. Rath, D. Pennachio, M. E. Flatté, P. M. Voyles, C. J. Palmstrøm, and P. A. Crowell, Phys. Rev. B 94 (2009) 235309.

[9] P. Bruski, Y. Manzke, R. Farshchi, O. Brandt, J. Herfort, and M. Ramsteiner, Appl. Phys. Lett. 103 (2013) 052406.

[10] Y. Fujita, M. Yamada, M. Tsukahara, T. Oka, S. Yamada, T. Kanashima, K. Sawano, and K. Hamaya, Phys. Rev. Applied 8 (2017) 014007.

[11] M. Yamada, F. Kuroda, M. Tsukahara, S. Yamada, T. Fukushima, K. Sawano, T. Oguchi, and K. Hamaya, NPG Asia Mater. 12 (2020) 47.

[12] K. Kudo, M. Yamada, S. Honda, Y. Wagatsuma, S. Yamada, K. Sawano, and K. Hamaya, Appl. Phys. Lett. 118 (2021) 162404.

[13] R. Weht and W. E. Pickett, Phys. Rev. B 60 (1999) 13006.

[14] I. Galanakis, P. H. Dederichs, and N. Papanikolaou, Phys. Rev. B 66 (2002) 174429.

[15] B. Balke, G. H. Fecher, H. C. Kandpal, C. Felser, K. Kobayashi, E. Ikenaga, J.-J. Kim, and S. Ueda, Phys. Rev. B 74 (2005) 104405.

[16] S. Wurmehl, G. H. Fecher, H. C. Kandpal, V. Ksenofontov, C. Felser, H.-J. Lin, and J. Morais, Phys. Rev. B 72 (2005) 184434.

[17] J. C. Slonczewski, J. Magn. Magn. Mater. 159 (1996) L1.

[18] Y. Yoshida, M. Kawakami, and T. Nakamichi, J. Phys. Soc. Jpn. 50 (1981) 2203.

[19] F. Kuroda, Ph. D. Thesis, Osaka University, 2020.

[20] H. Itoh, T. Nakamichi, Y. Yamaguchi, and N. Kazama, Trans. Jpn. Inst. Metals 24 (1983) 265.

[21] C. Jiang, M. Venkatesan, J.M.D. Coey, Solid State Commun. 118 (2001) 513.

[22] J. Karel, F. Bernardi, C. Wang, R. Stinshoff, N.-O. Born, S. Ouardi, U. Burkhardt, G. H. Fecher and C. Felser, Phys. Chem. Chem. Phys. 17 (2015) 31707.

[23] B. Deka, A. Srinivasan, R. K. Singh, B.S.D.Ch.S.Varaprasad, Y.K. Takahashi, and K. Hono, J. Alloys Compd. 662 (2016) 510.

[24] K. Nagai, H. Fujiwara, H. Aratani, S. Fujioka, H. Yomosa, Y. Nakatani, T. Kiss, A. Sekiyama, F. Kuroda, H. Fujii, T. Oguchi, A. Tanaka, J. Miyawaki, Y. Harada, Y. Takeda, Y. Saitoh, S. Suga, and R. Y. Umetsu, Phys. Rev. B 97 (2018) 035143.

[25] R. Y. Umetsu, H. Fujiwara, K. Nagai, Y. Nakatani, M. Kawada, A. Sekiyama, F. Kuroda, H. Fujii, T. Oguchi, Y. Harada, J. Miyawaki, and S. Suga, Phys. Rev. B. 99 (2019) 134414.

[26] T. Kubota, K. Kodama, T. Nakamura, Y. Sakuraba, M. Oogane, K. Takanashi, and Y. Ando, Appl. Phys. Lett. 95 (2009) 222503.

[27] T. Kubota, K. Kodama, T. Nakamura, Y. Sakuraba, M. Oogane, H. Naganuma, K. Takanashi, and Y. Ando, J. Magn. Soc. Jpn., 34 (2010) 100-106.

[28] M. Meinert, J-M. Schmalhorst, G. Reiss, and E. Arenholz, J. Phys. D: Appl. Phys. 44 (2011) 215003.

[29] K. Fukuda, M. Oogane, and Y. Ando, IEEE Trans. Magn. 53 (2017) 2600304.

[30] T. Tsuchiya, R. Kobayashi, T. Kubota, K. Saito, K. Ono, T. Ohhara, A. Nakao, and K. Takanashi, J. Phys. D: Appl. Phys. 51 (2018) 065001.

[31] T. Kubota, Y. Shimada, T. Tsuchiya, T. Yoshikawa, K. Ito. Y. Takeda, Y. Saitoh, T. J. Konno, A. Kimura, and K. Takanashi, Nanomaterials, 11 (2021) 1723.

[32] T. Tsuchiya, J. Okabayashi, and S. Mizukami, J. Magn. Magn. Mater. 540 (2021) 168437.

[33] K. Hamaya, H. Itoh, O. Nakatsuka, K. Ueda, K. Yamamoto, M. Itakura, T. Taniyama, T. Ono, and M. Miyao, Phys. Rev. Lett. 102 (2009) 137204.

[34] S. Yamada, K. Hamaya, K. Yamamoto, T. Murakami, K. Mibu, and M. Miyao, Appl. Phys. Lett. 96 (2010) 082511.

[35] K. Kasahara, K. Yamamoto, S. Yamada, T. Murakami, K. Hamaya, K. Mibu, and M. Miyao, J. Appl. Phys. 107 (2010) 09B105.

[36] K. Hamaya, T. Murakami, S. Yamada, K. Mibu, and M. Miyao, Phys. Rev. B 83 (2011) 144411.

[37] S. Yamada, J. Sagar, S. Honda, L. Lari, G. Takemoto, H. Itoh, A. Hirohata, K. Mibu, M. Miyao, and K. Hamaya, Phys. Rev. B 86 (2012) 174406.

[38] S. Yamada, K. Tanikawa, S. Oki, M. Kawano, M. Miyao and K. Hamaya, Appl. Phys. Lett. 105 (2014) 071601.

[39] S. Yamada, K. Kudo, R. Okuhata, J. Chikada, Y. Nakamura, and K. Hamaya, Appl. Phys. Express 10 (2017) 115802.

[40] K. Kudo, S. Yamada, J. Chikada, Y. Shimanuki, T. Ishibe, S. Abo, H. Miyazaki, Y. Nishino, Y. Nakamura, and K. Hamaya, Phys. Rev. B 99 (2019) 054201.

[41] K. Kudo, Y. Hamazaki, S. Yamada, S. Abo, Y. Gohda, and K. Hamaya, ACS Appl. Electron. Mater. 1 (2019) 2371.

[42] Y. Shimanuki, S. Yamada, A. Masago, T. Ishibe, K. Kudo, Y. Nakamura, and K. Hamaya, Phys. Rev. B 102 (2020) 054203.

[43] K. Kudo, S. Yamada, M. Yafuso, T. Kimura, V. K. Lazarov, and K. Hamaya, J. Alloys Compd. 854 (2021) 155571.

[44] K. Kudo, A. Masago, S. Yamada, L. S. R. Kumara, H. Tajiri, Y. Sakuraba, K. Hono, and K. Hamaya, Phys. Rev. B 103 (2021) 104427.

[45] S. Oki, S. Yamada, K. Tanikawa, K. Yamasaki, M. Miyao, and K. Hamaya, Appl. Phys. Lett. 103 (2013) 212402.

[46] S. Yamada, S. Honda, J. Hirayama, M. Kawano, K. Santo, K. Tanikawa, T. Kanashima, H. Itoh, and K. Hamaya, Phys. Rev. B 94 (2016) 094435.

[47] S. Yamada, S. Kobayashi, F. Kuroda, K. Kudo, S. Abo, T. Fukushima, T. Oguchi, and K. Hamaya, Phys. Rev. Mater. 2 (2018) 124403.

[48] Y. Takamura, R. Nakane, and S. Sugahara, J. Appl. Phys. 105 (2009) 07B109.

[49] Y. Takamura, T. Suzuki, Y. Fujino, and S. Nakagawa, J. Appl. Phys. 115 (2014) 17C732.

[50] Y. Nishino, M. Kato, S. Asano, K. Soda, M. Hayasaki, and U. Mizutani, Phys. Rev. Lett. 79 (1997) 1909.

[51] K. Kudo, S. Yamada, J. Chikada, Y. Shimanuki, Y. Nakamura, and K. Hamaya, Jpn. J. Appl. Phys. 57 (2018) 040306.

[52] T. Kubota, M. Oogane, S. Mizukami, H. Naganuma, Y. Ando and T. Miyazaki, J. Phys.: Conf. Ser. 266 (2011) 012096.

[53] K. Nikolaev, P. Kolbo, T. Pokhil, X. Peng, Y. Chen, T. Ambrose, and O. Mryasov, Appl. Phys. Lett. 94 (2009) 222501.

[54] V. Ko, G. Han, J. Qiu and Y. P. Feng, Appl. Phys. Lett. 95 (2009) 202502.

[55] V. Ko, G. Han, and Y. P. Feng, J. Magn. Magn. Mater. 322 (2010) 2989.

[56] S. Chadov, T. Graf, K. Chadova, X. Dai, F. Casper, G. H. Fecher, and C. Felser, Phys. Rev. Lett. 107 (2011) 047202.

[57] V. Ko, J. Qiu, P. Luo, G. C. Han, Y. P. Feng. J. Appl. Phys. 109 (2011) 07B103 (2011).

[58] Z. Q. Bai, Y. H. Lu, L. Shen, V. Ko, G. C. Han, and Y. P. Feng, J. Appl. Phys. 111 (2012) 093911.

[59] Z. Q. Bai, Y. Cai, L. Shen, G. C. Han, and Y. P. Feng, Appl. Phys. Lett. 102 (2013) 152403.

[60] I. Di Marco, A. Held, S. Keshavarz, Y. O. Kvashnin, and L. Chioncel, Phys. Rev. B 97 (2018) 035105.

[61] E. Şaşıoğlu, T. Aull, D. Kutschabsky, S. Blügel, and I. Mertig, Phys. Rev. Applied 14 (2020) 014082.

[62] I. Galanakis, Phys. Status Solidi RRL 15 (2021) 2100139.

[63] T. Aull, E. Şaşıoğlu, and I. Mertig, Appl. Phys. Lett. 118 (2021) 052405.

[64] B. Pradines, L. Calmels, and R. Arras, Phys. Rev. Applied 15 (2021) 034009.

[65] R. Knut, P. Svedlindh, O. Mryasov, K. Gunnarsson, P. Warnicke, D. A. Arena, M. Björck, A. J. C. Dennison, A. Sahoo, S. Mukherjee, D. D. Sarma, S. Granroth, M. Gorgoi, and O. Karis, Phys. Rev. B 88 (2013) 134407.

[66] T. L. Brown-Heft, J. A. Logan, A. P. McFadden, C. Guillemard, P. Le Févre, F. Bertran, S. Andrieu, and C. J. Palmstrøm, Phys. Rev. Mater. 2 (2018) 034402.

[67] S. Yabuuchi, I. Kitagawa, and T. Hamada, Extended Abstract of the 2010 International Conference on Solid State Devices and Materials, F-6-3, p.1120-1121.

[68] S. Yabuuchi and I. Kitagawa, Jpn. J. Appl. Phys. **53** (2014) 093004.